RAPID COMMUNICATION

High-speed and broad optical bandwidth silicon modulator*

Xu Hao(徐 浩), Li Xian-Yao(李显尧), Xiao Xi(肖 希), Li Zhi-Yong(李智勇), Yu Yu-De(俞育德)†, and Yu Jin-Zhong(余金中)

State Key Laboratory on Integrated Optoelectronics, Institute of Semiconductors, Chinese Academy of Sciences, Beijing 100083, *China*

(Received 4 June 2013; revised manuscript received 15 July 2013)

A high-speed silicon modulator with broad optical bandwidth is proposed based on a symmetrically configured Mach–Zehnder interferometer. Careful phase bias control and traveling-wave design are used to improve the high-speed performance. Over a broadband wavelength range, high-speed operation up to 30 Gbit/s with a 4.5 dB–5.5 dB extinction ratio is experimentally demonstrated with a low driving voltage of 3 V.

Keywords: optical modulators, integrated optics, optoelectronic device characterization

PACS: 42.82.–m, 42.79.Hp, 85.60.Bt **DOI:** 10.1088/1674-1056/22/11/114212

1. Introduction

Silicon-based photonic integrated circuits (Si-PICs) are emerging as a promising solution for chip-scale high-speed data communication with potentially low cost and low power consumption.[1,2] As a critical component in the Si-PIC, the depletion-mode Mach–Zehnder modulator (MZM) can offer high modulation speed, and it has experienced dramatic performance improvements over the past few years.[3,4] High-speed electro-optic modulation over 40 Gbit/s has been demonstrated for this kind of silicon modulator recently,[5–7] and it has been chosen as a critical component for Si-PICs[8,9] or used for the advanced modulation formats.[10,11] Owing to the relatively weak phase changes via carrier depletion, the proposed MZM was fabricated in an asymmetric Mach–Zehnder interferometer (MZI) with arms of different lengths, which could provide a proper phase bias at a certain wavelength to enhance the modulation. However, the use of the asymmetric MZI led to high sensitivity to ambient temperature fluctuations due to the large thermo-optic coefficient of silicon[12] and offered only a discrete operational wavelength range of a few nanometers or less. These properties make the asymmetric MZM unsuitable for application to wavelength and dense wavelength division multiplexing (WDM/DWDM) systems because they have the intrinsic requirement of a high optical bandwidth. Further, these properties also make unsuitable the integration of the asymmetric MZM with the light source as the laser chip with an accurate output wavelength is not available in high volumes, not to mention the wavelength drift caused by the environmental effects such as variations in ambient temperature and power supply voltage.[13] This has led to considerable interest in improving the stability of silicon optical modulators.[14–17]

Theoretically, a symmetric MZM is not sensitive to the change in temperature or operational wavelength, as its stability depends mainly on the variation in the characteristics of the coupler structure.[4] Therefore, the demand for high speed, high thermal tolerance, and broadband optical bandwidth for the silicon modulator can be fulfilled by a symmetrically configured MZM. However, due to the relatively long phase shifters necessary for both low-voltage driving and low-power control of the phase bias, the transmission-line (TL) effect is a critical issue that determines the high-speed performance of the modulator. In this paper, we present a silicon modulator with a broad optical bandwidth based on a symmetric MZI structure. Through careful control of the phase bias and the traveling-wave design, a high-speed electro-optic modulation of up to 30 Gbit/s with a low driving voltage of $V_{pp} = 3$ V is experimentally demonstrated over a broad wavelength range.

2. Device design and fabrication

Figure 1(a) shows the schematic view of the MZM and the phase shifter with periodically interleaved PN junctions. The MZM was fabricated into a symmetric MZI structure in a CMOS-compatible foundry. Multi-mode interferences (MMIs) and grating couplers were utilized for light splitting, combining and coupling in and out. When the segment width of the interleaved PN junctions is equal to the depletion thickness, a maximal phase shift per unit length could be achieved.[18] However, due to the limitation of the fabrication tolerances, the interleaved PN junctions were designed to have a short segment width of 300 nm in the case where

*Project supported by the National High Technology Research and Development Program of China (Grant No. 2012AA012202), the National Basic Research Program of China (Grant No. 2011CB301701), the Knowledge Innovation Program of the Chinese Academy of Sciences (Grant No. KGCX2-EW-102), and the National Natural Science Foundation of China (Grant Nos. 61107048 and 61275065).

†Corresponding author. E-mail: yudeyu@semi.ac.cn

© 2013 Chinese Physical Society and IOP Publishing Ltd

moderate doping concentrations of $N_A = 3 \times 10^{17}$ cm^{-3} and $N_D = 5 \times 10^{17}$ cm^{-3} were used.

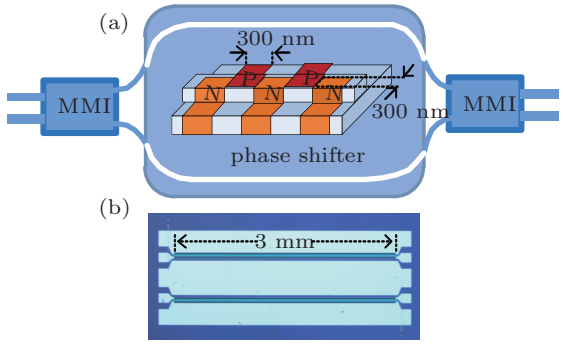


Fig. 1. (color online) (a) Schematic view of the MZM and the phase shifter with periodically interleaved PN junctions. (b) Microscope image of the MZM.

For the depletion-mode MZM, usually an extremely high driving voltage or a long phase shifter is necessary to achieve a π-phase difference between the phase shifters.[6] The ideal transfer function of an MZM can be described by means of a periodic cosine function

$$P_{\text{out}} = \frac{1}{2} P_{\text{in}} [1 + \cos(\varphi_0 + \Delta\varphi_{\text{m}})], \tag{1}$$

where P_{out} and P_{in} are the output and input optical power, φ_0 is the initial phase bias, and $\Delta\varphi_{\text{m}}$ is the modulated phase difference. At quadrature bias, the slope of P_{out} is steepest. Therefore, the control of the phase bias is essential for the enhancement of the electro-optic modulation with a low driving voltage. Several methods could be utilized to induce the phase bias, such as heating a phase shifter or injecting carriers into it. Since phase shifters should be formed in both arms to balance the carrier-induced optical loss, the low-power control of the phase bias can be realized by carrier depletion as well. The modulation efficiency $V_\pi L_\pi$ was estimated to be approximately 2 V·cm. Accordingly, a single phase shifter of 3 mm in length can provide a phase shift of 0.5π for phase bias or modulation by a driving voltage of only 3.3 V. An asymmetric MZM (AMZM), with the same phase shifter structure but an additional 100-μm-long strip waveguide in one arm, was fabricated for the extraction of the modulation efficiency of this phase shifter.

The high speed performance of the MZM mainly depends on the TL effect associated with the interaction between the microwave and the light wave.[19,20] Good velocity matching between the modulating microwave signal and the modulated optical signal will permit the phase modulation to accumulate effectively for high-speed operation, especially for an MZM with a long phase shifter. On an silicon-on-insulator (SOI) wafer with a 220-nm-thick top silicon layer and a 2-μm-thick buried oxide layer, a rib waveguide was designed to be 400-nm wide with a 90-nm high slab. The optical effective index was simulated using the full-vectorial beam-propagation method. As the grating couplers were designed for the transverse-electric (TE) mode, the effective index of the fundamental TE mode was considered only. Figure 2(a) shows the simulated results at different wavelengths around 1550 nm and the group index is approximately 3.78 for the rib waveguide. Based on the proposed circuit model,[21] both impedance matching and velocity matching were carefully considered. The width of the overlapping region in the interleaved PN junction was designed to be 300 nm in the center of the rib waveguide, which was intended to induce a low junction capacitance of $C_J = 274/\sqrt{0.92 - v}$ (fF/mm) at a certain reverse bias voltage (v) for the MZM. A 1-μm-thick aluminum coplanar waveguide (CPW) electrode was designed for the transmission of the driving signal. Both the width of signal line and the width of the gap of the CPW electrode were optimized to be 20 μm. Highly doped P+ and N+ regions were respectively defined 600 nm away from the edge of the rib waveguide. Figure 2(b) shows the curves of designed characteristic impedance Z_0 and effective index n_{eff} of the microwave of the MZM versus frequency. When the bias voltage is reduced from 0 V to −3 V, the Z_0 increases from 35 Ω to 45 Ω and the n_{eff} decreases from 4.0 to 3.4 which are around the group index of the rib waveguide.

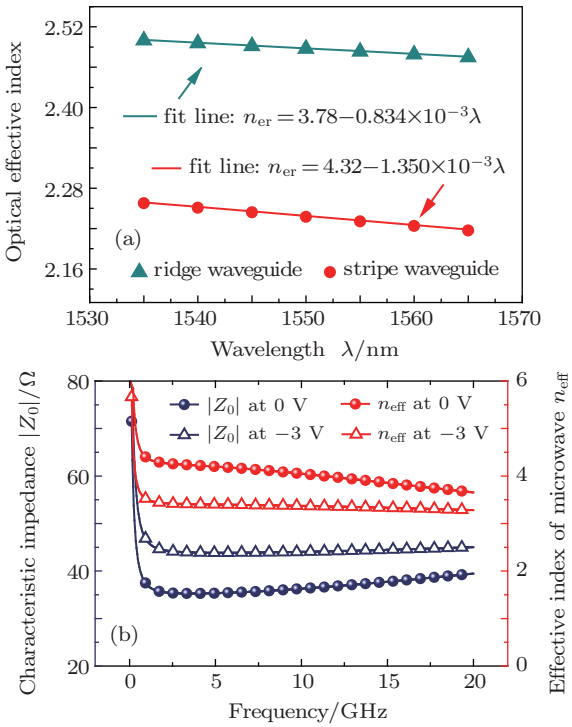


Fig. 2. (color online) (a) Optical effective indices versus wavelength of the rib waveguide and the strip wave guide. (b) Designed characteristic impedances and effective indices versus frequency of the MZM at bias voltages of 0 V and −3 V.

3. Measurement results and discussion

3.1. DC performance

The transmission spectra of the AMZM were measured in order to extract the modulation efficiencies of the phase shifter at different reverse-bias voltages. The phase shifters of the AMZM are 2-mm-long with an additional strip waveguide that is 100-μm-long and 400-nm-wide in one arm. Equation (1) shows the ideal transfer function of an MZM, in which the initial phase bias φ_0 for the proposed AMZM is expressed as

$$\varphi_0 = \frac{2\pi}{\lambda} n_{es} \Delta L, \tag{2}$$

where λ is the wavelength, n_{es} and ΔL are the effective index and the length of the strip waveguide, respectively. If only the first-order dispersion of the effective index is considered, the group index of the strip waveguide can be approximated by

$$n_{gs} = n_{es} - \lambda \frac{\partial n_{es}(\lambda)}{\partial \lambda} \approx n_{es} - k_s \times \lambda, \tag{3}$$

where k_s is the first-order dispersion constant. Figure 2(a) shows the values of simulated n_{es} at wavelengths around 1550 nm, and the n_{gs} and the k_s were calculated to be 4.32 nm^{-1} and -1.35×10^{-3} nm^{-1}, respectively. Therefore, the transfer function of the proposed AMZM at a bias voltage (V_{bias}) is rewritten as

$$P_{out} = \frac{1}{2} P_{in} \left\{ 1 + \cos \left[2\pi \Delta L \left(\frac{n_{gs}}{\lambda} - k_s \right) + \Delta\varphi_m(v_{bias}) \right] \right\}. \tag{4}$$

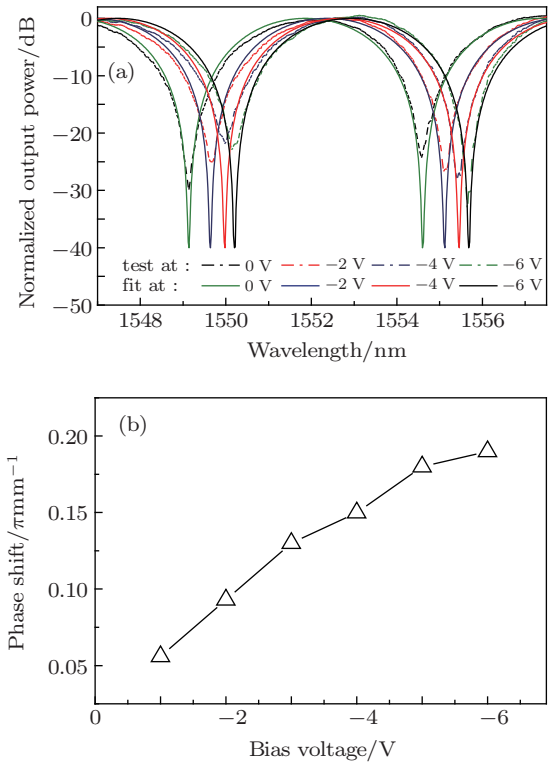


Fig. 3. (color online) (a) Normalized output powers versus the wavelength of the AMZM. (b) Extracted phase shift versus bias voltage.

Accordingly, the group index could be extracted from Eq. (4) by

$$n_{gs} = \frac{\lambda_{min}\lambda_{max}}{\Delta L \text{FSR}(\lambda)}, \tag{5}$$

where the free spectrum range (FSR) is the spectral periodicity of the MZM in a certain wavelength range around λ, and λ_{max} and λ_{min} represent the spectral positions of the transmission minima and maxima adjacent to the wavelength λ, respectively. Figure 3(a) shows the measured transmission spectra and those calculated by Eq. (4). Excellent curve-fitting has been achieved by setting $n_{gs} = 4.4$, $k_s = -1.3553 \times 10^{-3}$ nm^{-1} and $\Delta\varphi_0(0\text{ V}) = 0$. The phase shifts at different reverse bias voltages were extracted by fitting the measured curves and are shown in Fig. 3(b).

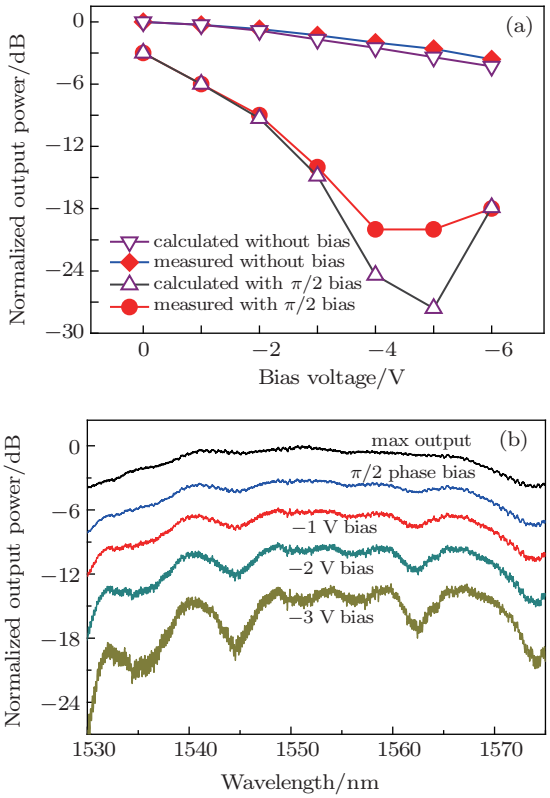


Fig. 4. (color online) (a) Normalized output powers of the MZM versus bias voltage for the cases of different phase biases. (b) Measured transmission spectra versus wavelength of the MZM.

For the symmetrically configured MZM with 3-mm-long phase shifters, the transmission spectra can be calculated using Eq. (4) as well. Figure 4(a) shows the curves of output optical power versus bias voltage for the cases with no phase bias and with a $\pi/2$ phase bias at 0 V. It demonstrates that by applying a $\pi/2$ phase bias with a driving voltage of 3 V, the static ER can be raised from 1.7 dB to 11.9 dB, though with an additional 3-dB optical loss. The measured result shows good agreement with that prediction. Figure 4(b) shows the measured transmission spectra of the MZM versus wavelength in the case with a $\pi/2$ phase bias, for which a reverse phase bias voltage lower than 4.5 V is needed. The 3-dB optical bandwidth of

the MZM is 39 nm, ranging from 1533 nm to 1572 nm, which almost covers the entire C band in the fiber-optic communication systems. The limitation of the optical bandwidth is mainly caused by the grating coupler utilized for coupling light in and out. With the reverse bias voltage increasing, the transmission spectra tend to be uneven and a few spectrum notches appear, which indicates the transmission spectra become sensitive at a low optical power level. The on-chip insertion loss of the MZM was measured to be ~ 9.5 dB by normalizing the maximum output spectrum to that of the grating couplers.

3.2. Dynamic performance

An on-wafer de-embedding technique[22] was applied to the extraction of TL characteristic parameters. The S parameters of the phase shifters with different lengths of 1000 μm and 750 μm were measured. The testing system, including the vector network analyzer, cables, probes, the bias-tee, and the DC block, was calibrated using the short-open-load-through calibration method on an impedance standard substrate. Figures 5(a)–5(c) show the test characteristic impedances, the effective indices of the microwave and the attenuation constants of the MZM and that calculated by the proposed circuit model.[21] The measurements indicate that the junction capacitance is $C_{\rm J} = 360/\sqrt{0.92 - v}$ (fF/mm), which is 30% higher than the designed value. It is believed that this discrepancy results from the fact that the overlapping region of the interleaved PN junctions spreads across the entire rib waveguide by diffusion. When the driving voltage changes from 0 V to −3 V, the Z_0 varies from 30 Ω to 40 Ω, the $n_{\rm eff}$ is in a range from 4.5 to 3.5 and the attenuation constant with a −3 V bias decreases to approximately half that without a bias. These parameters were characterized in a frequency range from 40 kHz to 15 GHz, the extraction at higher frequency is disturbed by the spectrum notch of the measured S-parameters which may result from the half-wavelength resonance.[23] Figure 5(d) shows the measured electro-optic (E/O) modulation response of the MZM against frequency. A response notch around 13 GHz appears which is mainly caused by the driving signal resonation. The 3-dB E/O bandwidth is approximately 14 GHz for the MZM with a low bias voltage of −1.5 V.

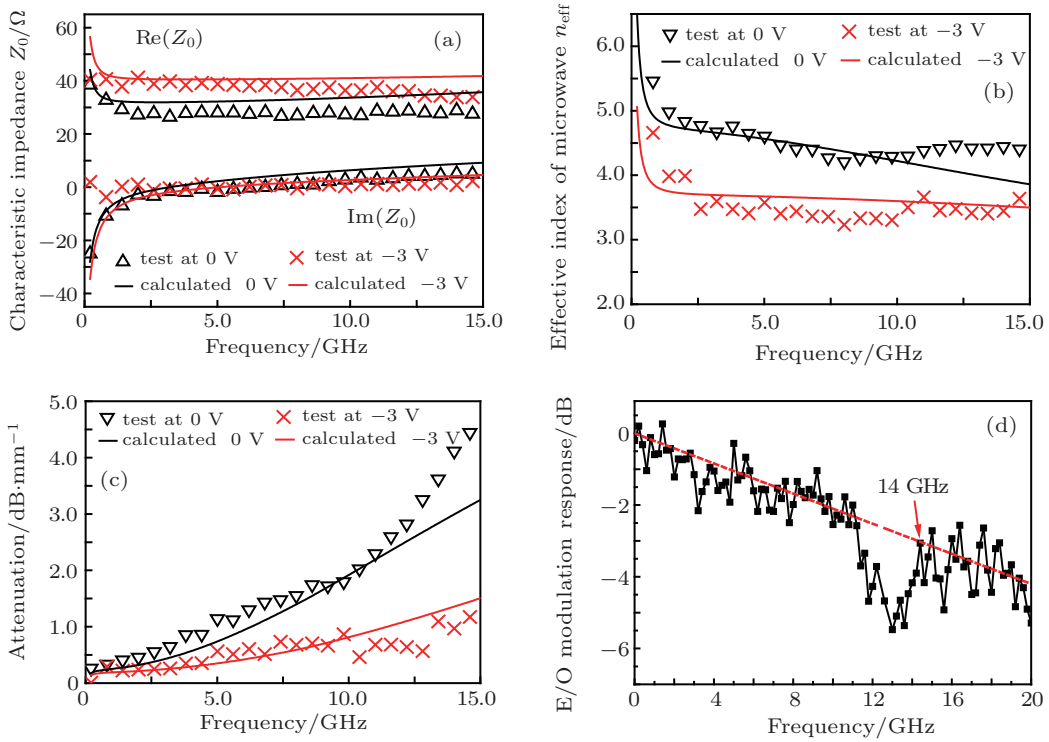


Fig. 5. (color online) Measured and calculated frequency-dependent TL parameters of the MZM at 0 V and −3 V: (a) characteristic impedances, (b) effective indices of microwave, (c) attenuation constants. (d) Measured E/O modulation response of the MZM at a bias of −1.5 V.

Optical eye diagrams were measured to demonstrate the high speed performance of the MZM by using a 30-Gbit/s non-return-to-zero pseudorandom binary sequence (PRBS) signal with a pattern length of $2^{31} - 1$. The phase difference between the two arms was set to be $\pi/2$ by applying a reverse bias voltage to one phase shifter. The PRBS signal was set to have 3-V peak-to-peak amplitude and was biased at −1.5 V to drive the other phase shifter of the MZM. A standard 50-Ω SMA terminal resistance and a DC block were both used as a termination load. A continuous-wave laser beam was coupled into the

MZM through a grating coupler. From the grating coupler on the other side, the modulated optical signal was amplified by erbium-doped fiber amplifier and detected by the optical module of a Tektronix digital oscilloscope. Figures 5(a)–5(d) show the output eye diagrams measured at different wavelengths from 1545 nm to 1565 nm. An extinction ratio (ER) of over 4.5 dB was measured over this broad wavelength range.

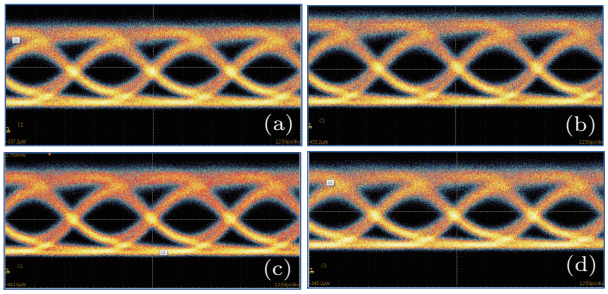


Fig. 6. (color online) The 30 Gbit/s eye diagrams measured at different wavelengths. (a) $\Lambda = 1545$ nm, ER = 4.5 dB, (b) $\Lambda = 1550$ nm, ER = 5.1 dB, (c) $\Lambda = 1560$ nm, ER = 5.5 dB, and (d) $\Lambda = 1565$ nm, ER = 4.7 dB.

4. Conclusions

In this paper, we present a high-speed silicon modulator with broad optical bandwidth. The phase-shifter based on the interleaved PN junctions is fabricated in a symmetrical MZI structure. The 30-Gbit/s electro-optical modulations with almost no additional bias power consumption are experimentally demonstrated over a broad wavelength range. Owing to its intrinsic property of being insensitive to change in temperature or operational wavelength, the silicon electro-optic modulator proposed has potential in more practical applications.

References

[1] Haurylau M, Chen G Q, Chen H, Zhang J D, Nelson N A, Albonesi D H, Friedman E G and Fauchet P M 2006 *IEEE J. Sel. Top. Quantum Electron.* **12** 1699

[2] Miller D A B 2009 *Proc. IEEE* **97** 1166

[3] Zhou L, Li Z Y, Xiao X, Xu H H, Fan Z C, Han W H, Yu Y D and Yu J Z 2011 *Chin. Phys. Lett.* **28** 074204

[4] Reed G T, Mashanovich G, Gardes F Y and Thomson D J 2010 *Nat. Photonics* **4** 518

[5] Thomson D, Gardes F, Fedeli J, Zlatanovic S, Hu Y, Kuo B, Myslivets E, Alic N, Mashanovich G and Reed G 2012 *IEEE Photon. Technol. Lett.* **24** 234

[6] Dong P, Chen L, Xie C, Buhl L L and Chen Y K 2012 *Opt. Express* **20** 6163

[7] Xiao X, Xu H, Li X Y, Hu Y T, Li Z Y, Chu T, Yu Y D and Yu J Z 2013 *Opt. Express* **21** 4116

[8] Kim G, Park J W, Kim I G, Kim S, Kim S, Lee J M, Park G S, Joo J, Jang K S, Oh J H, Kim S A, Kim J H, Lee J Y, Park J M, Kim D W, Jeong D K, Hwang M S, Kim J K, Park K S, Chi H K, Kim H C, Kim D and Cho M H 2011 *Opt. Express* **19** 26936

[9] Chen L, Doerr C, Dong P and Chen Y 2011 *Opt. Express* **19** B946

[10] Dong P, Chen L, Xie C, Buhl L L and Chen Y K 2012 *Opt. Express* **20** 21181

[11] Dong P, Xie C, Chen L, Buhl L L and Chen Y K 2012 *Opt. Express* **20** B624

[12] Cocorullo G and Rendina I 1992 *IEEE Electron. Lett.* **28** 83

[13] DeCusatis C and Jacobowitz L 2007 *Sarnoff Symposium IEEE*, April 30–May 2, 2007, Nassau Inn, Princeton, NJ, pp. 1–5

[14] Teng J, Dumon P, Bogaerts W, Zhang H, Jian X, Han X, Zhao M, Morthier G and Baets R 2009 *Opt. Express* **17** 14627

[15] Guha B, Gondarenko A and Lipson M 2010 *Opt. Express* **18** 1879

[16] Padmaraju K, Chan J, Chen L, Lipson M and Bergman K 2012 *Opt. Express* **20** 27999

[17] Zhang X J, Feng X, Zhang D K and Huang Y D 2012 *Chin. Phys. B* **21** 124203

[18] Li Z Y, Xu D X, McKinnon W R, Janz S, Schmid J H, Cheben P and Yu J Z 2009 *Opt. Express* **17** 15947

[19] Walker R G 1991 *IEEE J. Quantum Electron.* **27** 654

[20] Kubota K, Noda J and Mikami O 1980 *IEEE Quantum Electron.* **QE-16** 754

[21] Xu H, Xiao X, Li X Y, Hu Y T, Li Z Y, Chu T, Yu Y D and Yu J Z 2012 *Opt. Express* **20** 15093

[22] Mangan A M, Voinigescu S P, Yang M T and Tazlauanu M 2006 *IEEE Trans. Electron Dev.* **53** 235

[23] Heymann P, Prinzler H and Schnieder F 1994 *Microwave Symposium Digest, IEEE MTT-S International*, May 23–27, 1994, San Diego, CA, USA, p. 1045